Hearing Research, 50 (1990) 145–162
Elsevier

HEARES 01471

Basilar membrane nonlinearity and its influence on auditory nerve rate-intensity functions *

Graeme K. Yates

Department of Physiology, The University of Western Australia, Nedlands, Western Australia

(Received 27 November 1989; accepted 13 June 1990)

Previous papers have shown that the shapes of rate-intensity functions of auditory nerve fibres vary with spontaneous rate (Sachs and Abbas 1974; Sachs et al. 1989; Winter et al. 1990; Yates et al. 1990), and that the variation is due to the nonlinear properties of the basilar membrane. This paper examines the basilar membrane nonlinearity and provides a semi-quantitative explanation for it in terms of previous models (Zwicker 1979; Patuzzi et al. 1989) and an analogue model. It thereby provides explanations for the shapes of the basilar membrane input-output curves and for the way in which they vary with trauma. The shapes of the neural rate-intensity functions are quantified and shown to be consistent with the low-threshold data of Geisler et al. (1985). Several nonlinear properties of the cochlea, such as recruitment, are also interpreted.

Dynamic range; Rate-intensity function; Outer hair cells; Basilar membrane nonlinearity

Introduction

Several authors have described a number of properties which differ significantly between auditory nerve fibres with differing rates of spontaneous activity (Sachs and Abbas, 1974; Palmer and Evans, 1980; Schalk and Sachs, 1980; Liberman, 1978; Winter et al., 1990)). It has been suggested (Sachs and Abbas, 1974; Sachs et al., 1989) that the origin of this variability lies in the nonlinear properties of the basilar membrane, but this has been disputed by others (Palmer and Evans, 1980). A previous paper from this laboratory (Winter et al., 1990) demonstrated the existence of a continuum of properties expressed in such fibres in the guinea pig auditory nerve. These properties, of threshold and rate-intensity (RI) shape, were strongly correlated with spontaneous rate across fibres. In a second paper (Yates et al., 1990) it was shown that this continuum was indeed strongly connected with the nonlinear properties of the basilar membrane (BM), with the threshold of each fibre determining how it would interact with that nonlinearity (Sachs et al., 1989). The present paper examines the nature of the BM nonlinearity, some properties of the neural RI functions and some psychoacoustical consequences of the interaction.

How the basilar membrane influences the shapes of the rate-intensity functions

Fig. 1 shows in diagrammatic form the fundamental idea, first proposed in its basic form by Sachs and Abbas (1974) and later in a more quantitative paper by Sachs et al. (1989), and given strong support by Yates et al. (1990), of how the nonlinearity in the BM input/output function influences the shape of the neural RI functions and extends the dynamic range of the cochlea. At its most sensitive frequency the BM input-output function apparently has three distinct regions: at low stimulus intensities it is linear with output

Correspondence to: Graeme K. Yates, Department of Physiology, The University of Western Australia, Nedlands, 6009, WA, Australia.

* Portions of this work were reported at the Boden Research Conference, Thredbo, New South Wales, Australia, February 1–3, 1989.

0378-5955/90/$03.50 © 1990 Elsevier Science Publishers B.V. (Biomedical Division)

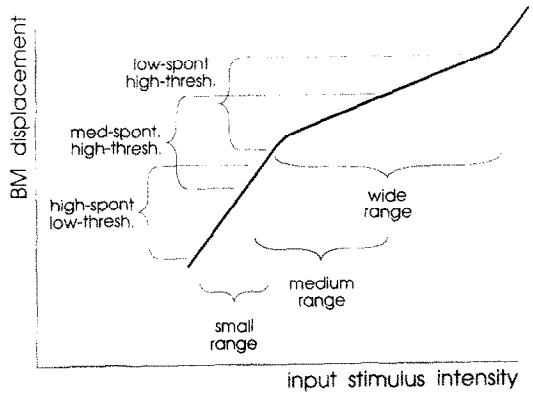

Fig. 1. The nonlinear basilar membrane input-output function, combined with a range of auditory nerve fibres of different thresholds, gives rise to the variety of rate-intensity functions observed. The three brackets to the left of the curve represent the dynamic ranges of three separate fibres with different sensitivities. The three brackets below the curve represent the corresponding input dynamic ranges for each of the three fibres (see also Sachs et al., 1989).

growing in direct proportion to input intensity, at intermediate intensities it has a power-law form with a flat slope, and at higher intensities it becomes linear again. This behaviour has been inferred in part from direct measurements of BM motion (Rhode, 1971; Sellick et al., 1982; Robles et al., 1986; Johnstone et al., 1986) and in part from a comparison of neural RI functions at characteristic frequency (CF) and tail frequencies (Yates et al., 1990). The two techniques agree well, both quantitatively and qualitatively. Measurements of RI functions at frequencies well below CF (the tail frequencies) for fibres with similar CFs demonstrate that different auditory-nerve fibres have different thresholds to identical BM displacements, with low-spontaneous fibres requiring greater BM amplitude to elicit a response than do high-spontaneous fibres (Liberman, 1978; Winter et al., 1990). The variation in threshold causes individual fibres to respond over different displacement ranges of the BM input-output function and, as a direct consequence, to exhibit different RI functions at CF (Sachs and Abbas, 1974).

Highly sensitive fibres, those which begin to increase their rate of action potential (AP) generation at very small displacements of the BM, are fully saturated before the initial linearity limits of the BM are reached and consequently they generate RI functions which are simple sigmoid-shaped curves. The dynamic ranges of such units are small, of the order of 20 dB from threshold of response to saturation. Fibres of intermediate sensitivity, those which do not respond until the BM motion increases by a factor of approximately 2–6 times more than the threshold displacement of the most sensitive units, exhibit similar RI shapes until about 10 dB above threshold, where they enter the transitional region of the BM input-output response. Above this intensity they increase their firing rate much more slowly as the BM increases its displacement by only (in the guinea pig) 0.2–0.25 dB for every dB increase in stimulus intensity (Yates et al., 1990). The dynamic ranges of these fibres are greater, typically 50–60 dB or more. Finally, fibres with still higher thresholds, as much as 6–15 times higher than the most sensitive, begin to respond just as the BM enters the transitional region and hence they show almost straight RI responses. The dynamic ranges of this third group of units are at least as great as those of both the more sensitive types, and they may well continue to increase their firing rate up to as much as 120–140 dB sound pressure level (SPL).

The shape of the BM I/O function

The shape of the BM input-output (I/O) function was explained by Yates et al. (1990) in terms of a model proposed originally by Zwicker (1979, 1986) and for which Patuzzi et al. (1989) provided experimental support, identifying the outer hair cells as the major source of nonlinearity affecting the motion of the BM. We expand that model here and use it to develop an empirical description of the BM nonlinearity. A related, but significantly different, model has been examined by Mountain et al. (1983).

A simple analogue

Consider first a simple example of an electronic feedback circuit Fig. 2A (although a similar mechanical system would produce identical results). An amplifier of gain G has a copy of its output signal attenuated and coupled back to a summing junction at its input. The insertion gain of the attenua-

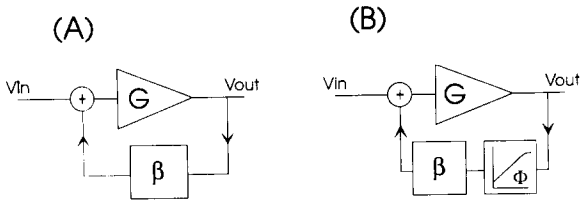

Fig. 2. Electronic model of active feedback acting to enhance gain. (A) shows a completely linear circuit which has a completely linear response. (B) As for A but with a saturating nonlinearity $\Phi(V_{out})$ included in the feedback loop. ($\Phi(V_{out})$ is the insertion gain of the element, its output is given by $\Phi \cdot V_{out}$). The feedback path is assumed to contain a bandpass filter which passes signals of the input frequency only.

tor, β, is such that the product βG is slightly less than unity. Analysis of such a circuit shows (see Brophy, 1983) that the gain is entirely linear (if its component parts are also linear) and is given by

$$G_{closed} = \frac{G}{1 - \beta G} \tag{1}$$

where G_{closed} is the overall closed-loop gain. If, however, the attenuator is preceded by a saturating gain element $\Phi(V_{out})$ (Fig. 2B) and a simple filter to permit feedback of only the fundamental component, then the feedback signal will be further attenuated at higher input intensities by the insertion gain of the nonlinear circuit ($\Phi(V_{out})$). The closed-loop gain will then be

$$G_{closed} = \frac{G}{1 - \beta \Phi G} \tag{2}$$

Since the feedback gain is reduced, the overall gain G_{closed} will be reduced by a larger amount. Assuming a simple saturating I/O function for the nonlinear feedback element, i.e.,

$$\Phi(V_{out}) = \frac{A_{corner} \cdot V_{out}}{A_{corner} + V_{out}} \tag{3}$$

where A_{max} and A_{corner} are arbitrary parameters, leads to the following expression for the closed-loop gain as a function of intensity.

$$G_{closed} = \frac{G(V_{out} + A_{corner})}{A_{corner} + A_{out} - \beta G A_{corner}} \tag{4}$$

When this circuit is driven by a sinusoidal input signal, the I/O function is not available in analytic form and must be calculated by numeri-

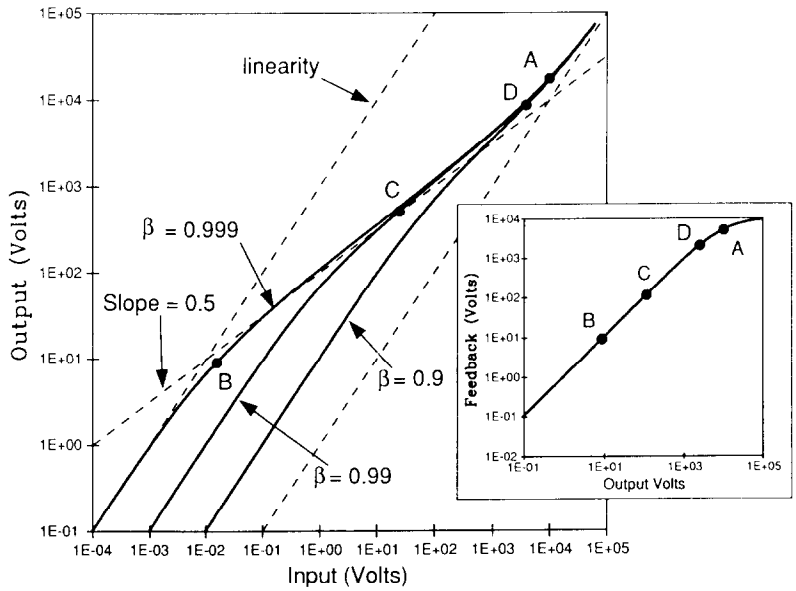

Fig. 3. Input-output function for the circuit of Fig. 2B for three values of β and assuming a simple hyperbolic saturation for the nonlinear element. Note that the abscissa covers a range of 9 orders-of-magnitude while the ordinate spans only 6 orders-of-magnitude. The inset shows the input-output function for the nonlinear element itself. Thus the abscissa of the inset is the same axis as the ordinate of the main chart. The points A, B, C and D in the two parts of the figure mark corresponding points. $G = 1$.

cal means. Substituting a sinusoidal waveform of various amplitudes into Φ and computing the amplitude of the fundamental component of the output voltage leads to the input-output function for the configuration of Fig. 2(B). It is plotted in Fig. 3 for $G = 1$, $A_{corner} = 10^4$, and three values of the feedback parameter β, 0.9, 0.99 and 0.999, which result in closed-loop gains of 20, 40 and 60 dB respectively. For any given value of β the input-output function is a strongly nonlinear function of intensity: it is linear at low input levels, nonlinear with a slope of approximately 0.5 at intermediate intensities, and then returns to a linear behaviour at the highest intensities. Different values of β change the low and intermediate-intensity gains but do not affect the high intensity responses.

The inset graph of Fig. 3 shows the response of the nonlinear element Φ itself, the abscissa being the output (from the amplifier) voltage and the ordinate being the feedback voltage. Thus, the ordinate of the main graph and the abscissa of the inset graph are the same. Notice that the input to the circuit varies over a dynamic range of 9 orders of magnitude but the output signal varies by only 6 orders of magnitude. Notice also that the nonlinear element in the feedback loop is subjected to signals which vary only over the reduced dynamic range of the output signal.

Causes of this behaviour

The behaviour of this circuit may be understood by considering separately the three input levels. (A) At very low input intensities the effect of Φ is small and the closed-loop gain reduces to that of Eq. 1. The response is a linear function of intensity with gain $1/(1 - \beta G)$. (B) At high intensities the nonlinearity is saturated and the amplitude of the feedback signal is constant, regardless of input level. The output amplitude then becomes independent of the feedback loop (the loop is essentially opened) and the overall gain approaches G. Again the response is linear. (C) It is between these two extremes that the circuit exhibits a nonlinear response as the gain of the feedback loop falls with increasing drive.

Both ends of the sloping region are determined by the saturation properties of the nonlinear element, but the effects are quite different for each end.

The upper corner, where the response approaches linearity again, is a consequence of the feedback gain approaching saturation. This is illustrated by the two points marked A in Fig. 3, which indicate corresponding points on the I/O curve of the nonlinear element and of the overall circuit. At this point the nonlinearity is rapidly reducing the feedback loop gain to a point where it is negligible and the amplifier is operating effectively open-loop.

The nature of the lower corner points, marked B, C and D on each of the three curves of Fig. 3, respectively, is more subtle, however. This transition occurs when the nonlinearity reduces the loop gain by an amount comparable with the magnitude of $1 - \beta G$. That is, when the nonlinearity results in a significant change in the magnitude of the denominator of Eq. 3. For example, consider the result of a reduction of just 0.2% in the feedback gain caused by the nonlinearity saturating to the extent of 0.2%. If the value of $1 - \beta\Phi G$ initially was 0.002 (resulting in an overall closed-loop gain of 500, or 54 dB), this would change to 0.004, reducing the closed-loop gain to 48 dB. Thus, a 0.2% fall in the insertion gain of the nonlinear element would reduce the closed-loop gain by 6dB. That is, the input-output response deviates from linearity at the lower intensities when the nonlinearity changes its gain by only a very small amount.

Thus, while the upper-intensity corner is fixed by the properties of the saturating nonlinearity, the location of the lower-intensity corner depends on the closed-loop gain and the form of the nonlinearity. If the closed-loop gain is reduced, by a change in β, say, the location of the lower-intensity corner will shift to higher intensities. The lower corner will, to some extent, track changes in the feedback gain and the general shape of the curve will be preserved. The curves for $\beta = 0.999$, 0.99 and 0.9 in Fig. 3 illustrate this. The low-intensity gain changes by 20 dB between each of these curves and the location of the corner points, B, C and D change by approximately the same amount. The upper corner is, of course, almost unaffected by changes in β.

In the cochlea

Referring these properties back to the cochlea and following Patuzzi et al. (1989), we equate the feedback path with the active process and the nonlinearity with the transduction mechanism in the outer hair cells (OHCs), that is, with the cochlear microphonic (CM) generator mechanism: the gates in the stereocilia. This suggests that the transition from low-intensity linearity to the flatter region in the I/O curves occurs when the nonlinearity of the OHC current transduction reduces the drive to the active process by a very small amount (Patuzzi et al., 1989). In contrast, the upper transition process, observed only by Sellick et al. (1982) (but see also Johnstone et al. 1986) would be a consequence of the more obvious saturation of the OHC currents. Furthermore, the reduced dynamic range to which the feedback nonlinear element is subjected corresponds with the reduced dynamic range to which the OHCs (and hence the inner hair cells, IHCs) are subjected during CF stimulation.

The nonlinear, intermediate portion of the I/O curve of Fig. 3 has a slope of 0.5, much steeper than observed in direct measurements of BM motion by Robles et al. (1986) and in our own derived BM curves which show a slope of about 0.2. This discrepancy could be accounted for if the saturation of the OHC current was more abrupt than simple hyperbolic, as indeed it appears to be (Patuzzi et al., 1989). In an attempt to derive an empirical description of the response, we tried some variations on the hyperbolic saturation which would cause a more abrupt transition. Numerical analysis (see Appendix) demonstrated that a similar hyperbolic saturation but with the independent variable raised to the fifth power would produce a close approximation to the derived BM I/O curves. Thus, we calculated the I/O functions for the electronic circuit of Fig. 2 using the following equation for the shape of the instantaneous transfer curve

$$\Phi(V_{out}) = \left[\frac{A_{corner} \cdot V_{out}^5}{A_{corner}^5 + V_{out}^5}\right]^{1/5} \qquad (5)$$

Numerical solution showed the resulting I/O curve for such a transfer function (Fig. 4) to have

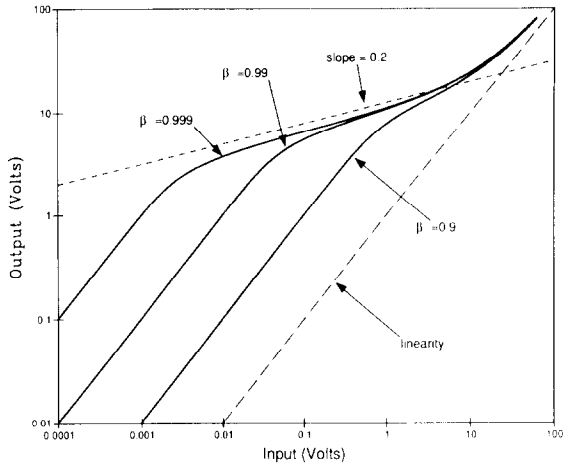

Fig. 4. The input-output response for the electrical circuit of Fig. 3 assuming a fifth-power hyperbolic saturation for the nonlinearity (Eq. 4). Three values of the feedback parameter β are shown, 0.999, 0.99 and 0.9, corresponding to closed-loop gains of 60, 40 and 20 dB respectively. The line marked with long dashes shows the open-loop gain of the circuit. The slope of the flatter region corresponds with a power law response with a slope of approximately 0.2 (short dashes). $G = 1$.

the same general shape as for the simple hyperbola (Fig. 3), but with a much flatter intermediate slope, very close to 0.2, and with a much more compressed dynamic range. In fact, the shape was very similar to that of the derived BM I/O curves. (More generally, numerical experimentation showed that using a power of $N > 2$ in place of the fixed value of 5 in Eq. 5 gave rise to curves of the form shown in Fig. 3 and 4 but with slopes close to $1/N$.) It should be understood that the choice of a 5th power hyperbola has no particular significance other than that it results in a transfer curve which has a more abrupt transition from linearity to saturation. Almost any other curve with similar saturation properties would do as well.

A full interpretation of BM motion in terms of the simple electronic analogue is complicated by the two-dimensional distribution of the travelling wave and of the active process. Whereas the electronic circuit is a one-dimensional analogue, the mechanical feedback in the cochlea appears to be spatially distributed (Diependal et al., 1986; Neely and Kim, 1983, 1986). One obvious consequence of this is that the BM motion might not be influenced as much by reductions in the feedback

loop gain as is implied by the simple model, because for any one stimulus intensity the various parts of the distributed nonlinearity are operating at different displacement amplitudes and hence at different degrees of saturation. Indeed, Mössbauer measurements of the BM and the observed RI functions both suggest that the minimum BM slope of 0.2 appears to be reached only at stimulus frequencies at or above CF; lower stimulus frequencies show less nonlinearity.

Quantitative analysis of neural rate-level curves

We now proceed to a quantitative analysis of neural RI functions for each of the three spontaneous-rate categories of fibre. The basis is similar to the analysis provided by Sachs et al. (1989) but here we consider each fibre classification separately and demonstrate that the accuracy of the description provided is best for high-spontaneous fibres and poorest for very low-spontaneous fibres.

High-spontaneous rate fibres

Yates et al. (1990) showed that the tail-frequency RI functions are well described by a simple saturation, with the square of the stimulus pressure as the independent variable (Sachs and Abbas, 1974, use a similar equation with an exponent of 1.77). The BM input-output function is linear at these frequencies (Sellick et al., 1982; Robles, et al., 1986) and so the neural RI functions must reflect nonlinearities which act after the BM motion. Since the BM motion at CF is also linear for low stimulus intensities, it is likely that the RI functions at CF are similar in shape to those at tail frequencies, and in fact this was observed (Yates et al., 1990).

The equation found by Yates et al. to describe the tail-frequency RI functions for most fibres and the RI functions at CF for high-spontaneous fibres is reproduced here for convenience.

$$R = A_0 + \frac{A_1 \cdot p^2}{A_2^2 + p^2} \qquad (6)$$

where...

R is the rate of AP generation

p is the sound pressure expressed in linear units

A_0 is the spontaneous firing rate, in APs/second

A_1 is the difference between the maximum AP rate and spontaneous, i.e., the maximum change in AP rate.

A_2 is the stimulus sound pressure at which the AP rate has increased by $A_1/2$ above spontaneous. It is a measure of fibre sensitivity to the applied stimulus.

The parameters A_0, A_1, and A_2 are assumed to vary from fibre to fibre and A_2 is assumed also to vary with stimulus frequency (as a consequence of the frequency selectivity of BM motion). This equation is similar to that used by Sachs et al. (1989) but uses an exponent of 2 rather than 1.77 as used by them. We used a nonlinear least-squares curve fitting program to adjust the parameters for each high-spontaneous fibre and found that suitable, consistent, values were obtainable for all such units at CF. (The same curve-fitting program was used to define all the smooth curves shown in Yates et al., 1990.) Fig. 5(A) shows an example of the quality of the represention achieved using Eq. 6, which generally describes the data very well. The lower panel shows the distribution of the residuals, i.e., the differences between the observed points and the fitted curve: individually they show no significant deviations from a random distribution about zero. As a further check on the quality of the fit, the dashed lines show the one-standard-deviation limits for the residuals under the assumption that the AP generation process obeys a Poisson distribution. If this were so, 76% of the residuals should lie within the boundaries and 23% outside. In fact, almost all lie inside, suggesting that the standard deviation is less than that for a Poisson process. (Geisler et al., 1985 show that the standard deviation of neural interspike intervals is equal to the mean value (i.e., the governing distibution is Poisson) for rates up to approximately 30/s and falls for faster rates. Teich and Khanna (1985) show that the number of APs occuring in a given time follows a distibution for which the variance is directly proportional to the mean, i.e., the standard deviation is proportional to the square-root of the mean, again indicating a Poisson process for low AP rates.)

Close examination, however, did reveal that many such high-spontaneous fibres, especially those with slightly higher (by 3–5 dB) thresholds than the typical, show small deviations from the calculated curve near the upper corner of the RI function. Typically, the observed firing rates had a tendency to lie slightly below the curve just where it began to saturate. Fig. 4 of Yates et al. (1990) is a good example of this: many of the RI functions therein fall just under the fitted curve, near the saturation point. We attribute this to the BM nonlinearity which departs from linearity just above this intensity. That is, many fibres which we would classify as being of the saturating RI type do in fact show signs of sloping saturation when compared in detail with the fitted curves. In spite of this, the description provided by Eq. 6 is, for most quantitative purposes, a very satisfactory description of the RI functions for high-spontaneous fibres.

Fig. 5D shows a RI function recorded from the same fibre at a tail frequency. Again the solid line is Eq. 6 with the parameters A_0, A_1 and A_2 adjusted according to the least-squares criterion. The description is also very good, with the residuals being distributed in a manner similar to the CF response.

Medium-spontaneous rate fibres

Auditory-nerve fibres with medium rates of spontaneous activity (in the range 0.5–18/s) typically exhibit RI functions of the sloping-saturation type (Sachs and Abbas, 1974; Winter et al. 1990). Sachs and Abbas, Sachs et al. (1989) and Yates et al. have shown that these RI functions are quantitatively consistent with the nonlinearity in the basilar membrane input-output function. In this section we now show that the RI functions for medium-spontaneous rate fibres may in many cases be well described by combining the description for high-spontaneous fibres with an empirical equation for the BM input-output function. A similar conclusion has previously been reached for cat data by Sachs et al. (1989).

The typical BM derived input-output function shows an initial linear region which rather abruptly changes into a power-law response with a slope of 0.2. To approximate this behaviour, and based on the modelling results of Fig. 4, we might assume an equation of the form

$$d = A_2 \left[\frac{A_3^4 \cdot p^5}{A_3^4 + p^4} \right]^{1/5} \tag{7}$$

where

d is the displacement of the basilar membrane at a given point

p is the input stimulus pressure

A_2 is an overall scaling factor.

A_3 is the stimulus pressure at which the BM nonlinearity becomes evident in the curves.

This function is similar to, but not identical with, the function used by Sachs et al. and has the form required to match approximately the derived BM I/O curves: at low intensities it reduces to $A_2 \cdot x$ while at high intensities it becomes $(A_2 A_3^{4/5}) \cdot x^{1/5}$. The stimulus intensity at which it changes from linear to a slope of 0.2 is A_3. Note that this equation does not attempt to model the very high intensity region shown in Fig. 1 and above the point A in Fig. 3.

This equation is combined with Eq. 6 above to produce an empirical description of the neural rate-level curves. Eq. 7 describes the relationship between stimulus intensity and BM displacement while Eq. 6 describes the relationship between BM displacement and neural discharge rate. Thus, substitution of d in Eq. 7 in place of p of Eq. 6 leads to an equation relating neural discharge rate to stimulus SPL. This should be capable of describing all of our RI data with only one extra parameter: the slope of the power-law region which we have so far taken as being exactly 0.2. It would be unlikely that all BM locations in all guinea pigs have exactly this slope, so accurate matching of theory to data may be possible only if it is adjustable. We accordingly denote this as parameter A_4 and arrive at the following equations to describe the AP rate as a function of sound pressure...

$$R = A_0 + \frac{A_1 \cdot d^2}{A_2^2 + d^2} \tag{8}$$

and

$$d = \left[\frac{A_3^{(1/A4-1)} \cdot p^{1/A4}}{A_3^{(1/A4-1)} + p^{(1/A4-1)}} \right]^{A4} \quad (9)$$

where

A_0 is the fibre spontaneous rate

A_1 is the maximum increase in firing rate, i.e., the maximum firing rate minus the spontaneous rate

A_2 represents the sensitivity of the nerve fibre, including the BM sensitivity. For the linear BM case (tail frequencies or saturating fibres at CF) it is the same as parameter A_2 in Eq. 6 while for the medium-spontaneous rate fibres it represents the product of A_2 of Eq. 6 and A_2 of Eq. 7.

A_3 is the sound pressure at which the BM changes from low-level linear to nonlinear behaviour

A_4 is the exponent of the power-law slope in the nonlinear region.

The same nonlinear parameter-estimation computer program was used to adjust the five parameters for each of the sloping-saturation RI functions recorded in the study by Winter et al. (1990). Fig. 5B shows the typical quality of representation provided by the fit for medium-spontaneous fibres stimulated at CF.

The lower panel of Fig. 5B again plots the residuals and the dotted lines mark the one-standard-deviation boundary for the residuals under the assumption that the AP occurrence times are governed by a Poisson process. Typically, the parameters provided an excellent description of the data although the values obtained for A_4, the slope of the nonlinear region, were sometimes larger than the value of 0.2 found by Yates et al. from direct comparison of CF and tail-frequency responses. The reason for this is not clear: the derived BM-response method of Yates et al. gave slopes which were quite consistently around 0.2 for CF responses, but the curve-fitting process sometimes produced larger values in the range 0.25–0.35. The most complete data of Robles et al., (animal Mo33, chinchilla) show a slope of 0.2 sustained over a very wide range of intensities and our own considerable volume of results from derived BM responses gave slopes clustering tightly around 0.2. Sachs et al. (1989) routinely used a value of 0.33 for their analysis of cat data, quoting Rhode (1971) and Robles et al. (1986) for direct measurements using the Mössbauer technique. Species differences could account for some variation here.

Experimentation with numerical modelling showed that saturation of the IHC response at very high stimulus intensities, so far not considered here, would lead to an additional flattening of the RI function, and that the curve-fitting process would interpret this as a steeper power-law slope coupled with a lower maximum AP rate. Consequently, we believe the derived BM input-output functions are the correct analyses and that the estimates for A_4 from Eq. 9 are slightly in error. This conclusion is supported by three observations: (a) the nearer the RI response was to saturating, (that is, the lower the thresholds were) the closer was the slope to 0.2, (b) forcing a slope of 0.2 for the parameter A_4 produced curves which modelled the observations accurately for all but the very highest-intensity stimuli and gave RMS residual values within 10% of the free-parameter fits, and (c) constructing derived BM I/O curves (Yates et al. 1990), which should factor out similar IHC saturation of both CF and tail-frequency responses, almost invariably gave slopes of 0.2.

Fig. 5(E) shows a typical fit to the tail-frequency RI function for the fibre of Fig. 5(B). The fitted function in this case suggests the maximum firing rate to be greater than that implied by the CF data, but this is influenced heavily by one data point alone.

Fig. 5. Examples of curve-fitting to neural RI functions at CF for saturating (A), sloping saturation (B) and straight (C) RI types. The residuals (shown in the panels below each RI function) show no systematic biases. The dashed lines are the square-roots of the RI functions themselves, marking one standard deviation for a Poisson process. Evidently the observed standard deviations are somewhat smaller than Poisson (see text) but are distributed approximately as expected. The lower panels (D, E and F) are the corresponding RI functions at tail frequencies for the same units. The numbers within the boxes are the least-squares values for the parameters $A_0 - A_4$. The parameters A_3 and A_4 were estimated in linear pressure units but have been converted here to dB SPL.

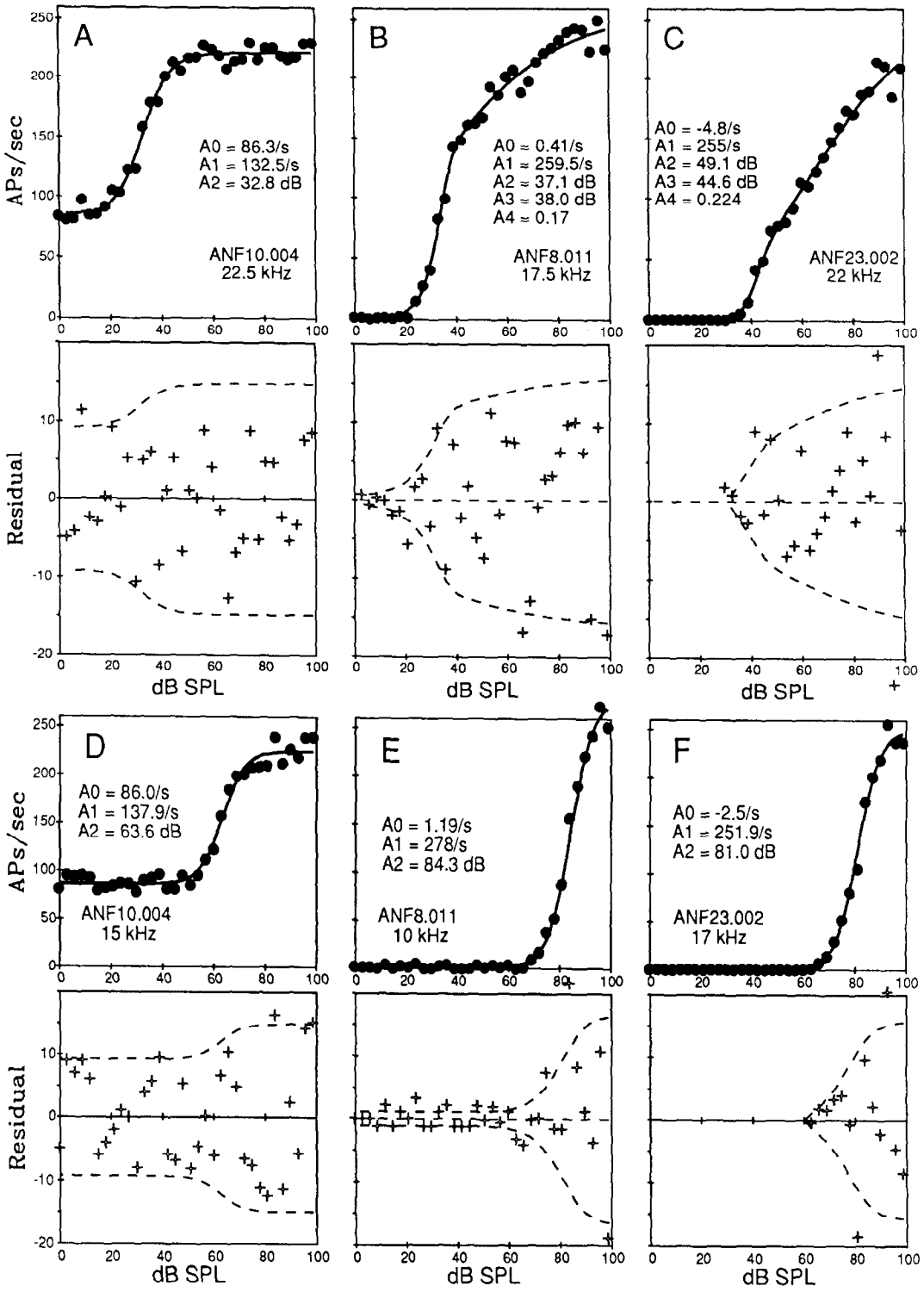
A
A0 = 86.3/s
A1 = 132.5/s
A2 = 32.8 dB
ANF10.004
22.5 kHz
B
A0 = 0.41/s
A1 = 259.5/s
A2 = 37.1 dB
A3 = 38.0 dB
A4 = 0.17
ANF8.011
17.5 kHz
C
A0 = -4.8/s
A1 = 255/s
A2 = 49.1 dB
A3 = 44.6 dB
A4 = 0.224
ANF23.002
22 kHz
APs/sec
Residual
dB SPL
D
A0 = 86.0/s
A1 = 137.9/s
A2 = 63.6 dB
ANF10.004
15 kHz
E
A0 = 1.19/s
A1 = 278/s
A2 = 84.3 dB
ANF8.011
10 kHz
F
A0 = -2.5/s
A1 = 251.9/s
A2 = 81.0 dB
ANF23.002
17 kHz

Low-spontaneous rate fibres

The fits for the low-spontaneous fibres, especially those with no measureable spontaneous activity, sometimes produced much larger values of A_4, ranging from 0.2–0.4. (The derived BM curves, however, still showed slopes of 0.2.) The tail-frequency data also were sometimes described inadequately by Eq. 8 and 9 and we attribute both discrepancies to the nonlinearity of the dc receptor potential within the inner hair cell, which we have not taken into account. The slope of the growth of the DC receptor potential is close to 2 at low intensities but saturates at higher intensities (Goodman et al., 1982: Patuzzi and Sellick, 1983). Since this nonlinearity is effectively in series between the BM displacement and the synaptic transduction, it is to be expected that it would manifest itself in the shapes of the RI functions at higher intensities.

Fig. 5C and 5F show a typical fit to RI data from a low-spontaneous fibre for CF and tail frequencies respectively.

For all fibres, it has proven convenient in practice to restrict the value of the A_4 parameter to a single value of 0.2. For the reasons argued above we find that estimated values of A_4 are in some error and we attribute this error to saturation of the receptor potential within the IHC. Fixing the value of A_4 results in RMS values of the residuals which are typically less than 10% greater than when A_4 is left to be optimised. This difference is small, the fitted curves appear visually to be just as convincing and the other parameters are only slightly shifted in their values. Consequently, we recommend that this approach be taken for all quantitative work since the value of 0.2 is justified on experimental grounds (Yates et al., 1990) and the improved consistency which results for the other parameters vindicates the approach.

RI functions at other frequencies

In Yates et al. (1990) we also applied the fitting procedure to two sets of data from other experiments which provided rate-level functions over a range of frequencies below and above CF, and a third set was taken from Patuzzi and Robertson 1988 (their Fig. 4). The curves so obtained clearly show the transition from linearity to nonlinearity as the stimulus frequency approaches and exceeds

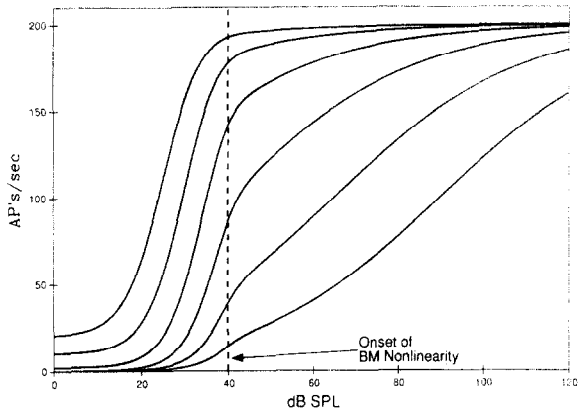

Fig. 6. Auditory-nerve CF rate-intensity functions calculated using typical values for the parameters A_0 through A_4. Each curve is calculated using assumed thresholds (parameter A_2) in 5 dB steps, covering a range of 25 dB. The spontaneous rate (A_0) has been adjusted arbitrarily to reflect the variation observed in experimental observations while the maximum firing rate ($A_0 + A_1$) has been held constant. The basilar membrane nonlinear slope (parameter A_5) has been held at 0.2. Note that these curves do not attempt to model the upper-intensity linear region, nor do they take any account of saturation of IHC receptor currents.

the CF (see Yates et al., 1990, Figs. 2 and 3, and also Sachs and Abbas, 1974, Figs. 4 and 6). It is known that unit rate-intensity functions flatten their slope at or above CF (Sachs and Abbas, 1974) and our interpretation of the derived BM I/O curves confirms Sachs and Abbas' explanation of why some units change slope at CF while others change slope only above CF. Rate-level functions for high-spontaneous, low-threshold units will show saturating behaviour for frequencies up to CF and then will progress through sloping saturation to straight RI functions for higher frequencies. Sloping saturation fibres will show saturating behaviour almost up to CF, sloping saturation near to CF and straight RI functions beyond. Finally, straight fibres will be saturating well below CF, will become sloping saturation just below CF and will become straight at and above CF.

Further examples of the fits obtained may be seen in Yates et al. (1990).

Variability of rate-intensity functions

We believe that almost the entire range of shapes seen in RI functions may be explained as the interaction between BM displacement and

auditory-nerve activity (Eq. 8), the nonlinear BM I/O curve (Eq. 9) and a variation in nerve thresholds. It is only for fibres of very high threshold that the quantitative relationship of Eq. 9 breaks down and this, we believe, is due to saturation of the IHCs.

CF rate-intensity responses are steep and saturate rapidly if and only if the fibre threshold is low (in which case the spontaneous rate will be high). Higher threshold units will show the same form of RI function at lower intensities but will be flatter at the higher intensities and may not reach saturation at all. All units will show flattening of their rate-level functions above CF (Sachs and Abbas, 1974). The apparently lower saturation discharge-rate above CF is simply a consequence of the flatter slope: if the unit could be driven hard enough it would saturate at the same firing rate regardless of stimulus frequency.

In order to illustrate the range of RI function shapes which are possible, several such functions were calculated using Eq. 8, Eq. 9 and typical values of the parameters A_0–A_4 (Fig. 6). No account was taken of possible saturation effects. The sensitivities of the 'synapses' in the calculations were varied over a range of 25 dB in 5 dB steps while the BM parameters and the maximum firing rate were maintained constant. (An artifical variation of spontaneous rate, A_0, with synapse threshold was added for realism.) The curves show the idealised variation of RI functions with threshold and illustrate the continuum of RI functions now described. The highest spontaneous-rate responses show the saturating responses typical of only a few of the most sensitive fibres. The next two curves show responses typical of the majority of high-spontaneous fibres: responses which may be classified as saturating but which, when compared accurately with Eq. 6, show definite signs of sloping-saturation. The third and fourth curves show responses typical of the majority of sloping-saturation fibres. The last curve is similar to many of our straight RI fibres, but many such functions recorded also showed a more marked saturation at high stimulus intensities, consistent with the suggestion that they are being affected by saturation of the IHCs.

Sachs and Abbas (1974) show a similar set of curves calculated with parameters they found appropriate to the cat auditory nerve. While the general shapes are similar, especially for the low-threshold model fibres, their modelled RI functions for the higher-threshold fibres are less straight than our modelled and observed curves. Our own calculations tell us this is because of the choice of parameters, particularly of the power-law slope parameter which they take as 0.33.

The shape of the rate-intensity curves at low stimulus intensities

Eq. 6 defines the relationship between the SPL and the firing rate of the nerve fibre stimulated at a tail frequency. The same function also describes the RI functions at CF for fibres of high sensitivity and spontaneous rate, and for medium-spontaneous and some low-spontaneous fibres at low firing rates. The general accuracy of these equations has been demonstrated over the full range of firing rates for all RI functions of saturating type, but has not been examined in great detail at the foot of the curves, close to threshold.

Geisler et al. (1985), measured near-threshold responses of cat auditory nerve fibres with great accuracy and concluded that the responses of low-spontaneous and high-spontaneous fibres were inherently different. They calculated slopes of the RI functions for the two types of fibres and showed that the low-spontaneous fibres had much flatter slopes close to threshold, resulting in some ambiguity in the definition of threshold for these fibres. Using their shape threshold definition, Geisler et al. calculated that the low-spontaneous fibres had thresholds which were only some 5 dB less sensitive than similarly defined thresholds for the high-spontaneous fibres and emphasised the small differences between the two when measured in this way.

We have claimed that our descriptions of the RI functions hold for most fibres near threshold, so it is important to establish the relationship between our Eq. 6–9 and the behaviour described by Geisler et al. If their data cannot be reconciled with our analysis then we must question the degree to which Eq. 6–9 may be universal.

We begin by assuming that, since we are considering only low stimulus levels, most fibres may

be described by Eq. 6 and by noting that under such low-intensity stimulation Eq. 6 reduces to

$$R_{\text{Thresh}} = A_0 + \frac{A_1 \cdot p^2}{A_2^2} \tag{10}$$

where R_{Thresh} is the AP rate at near-threshold stimulus intensities and A_0, A_1, and A_2 have the meanings defined above.

A simple replacement of the independent variable, by defining a new independent variable

$$u = p^2$$

results in

$$R_{\text{Thresh}} = A_0 + \left(\frac{A_1}{A_2^2} \cdot u\right) \tag{11}$$

which is a straight line.

Thus, if the low-intensity AP rate is plotted against the square of stimulus pressure, our description implies that a straight line should result for fibres of all high, medium and most low spontaneous rates. Fig. 7, (A) and (B), show original data from Geisler et al. Fig. 1 replotted on a new abscissa scale, the original dB scale having been converted to linear units and then squared. A straight line of best fit was then determined for each, using a least-squares criterion. The result is quite consistent for the high-spontaneous fibre (A) and even more convincing for the low-spontaneous fibre (B).The right-hand panels, (C) and (D), show the same data and lines plotted on the original dB SPL scale, and appear to be just as convincing in that form. More data on high-spontaneous fibres would give more confidence in the results, but on the available evidence it is clear that the description of the RI function presented here is quite compatible with Geisler et al's findings.

It is also consistent with the findings of Geisler et al. that low-spontaneous fibres showed steeper RI slopes at threshold (when plotted on a logarithmic rate scale) than did higher-spontaneous fibres. We have found that simple differentiation of Eq. 10, followed by some algebraic manipulation and the application of their definition of 'tracking

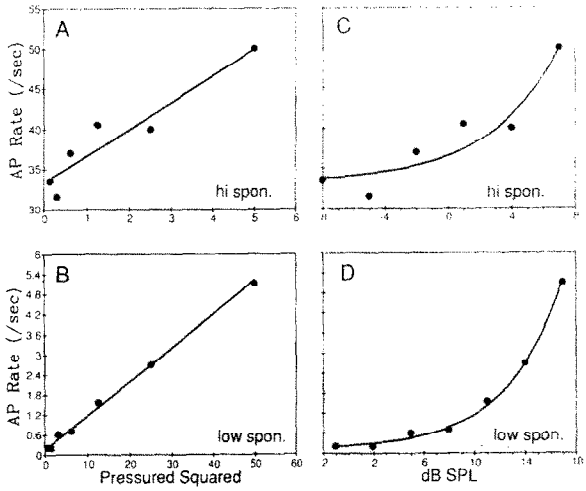

Fig. 7. Data from Geisler et al (1985) replotted on a new abscissa transformation, showing pressure-squared on a linear scale (A) for a high-spontaneous fibre and (B) for a low-spontaneous fibre. Both are well described by a straight line (solid line) demonstrating that Eq. 11 represents them accurately. (C, D). The same data replotted on the original coordinates along with the straight lines of (A) and (B).

threshold', produced estimates of slopes which were close to, although slightly higher than, the measured slopes of the original paper. Fig. 8 shows the calculated slopes plotted against the observed values, each as a function of spontaneous rate. It is clear that the magnitudes of the calculated slopes are comparable with the observed values and that the variation in slope with intensity is also typical of the data. The difference in absolute values might be attributable to the subjective method used by Geisler et al. to estimate their slopes and might disappear if the slopes were defined in terms of the straight-line description of Eq. 11. The important point is that there is no large difference between the observed slopes and slopes predicted from our analysis. Furthermore, the trend with spontaneous rate is accurately explained.

It is quite clear that variations in slope will exist when RI functions from fibres of different spontaneous rates are plotted on logarithmic coordinates, simply as a property of the logarithmic function: the addition of a constant value (the spontaneous rate) will reduce its slope. Our analysis and data suggest that the slope variation seen by Geisler et al. is a property of the logarithmic

function rather than of differences between the fibre RI functions. Thus, a fibre of exactly zero spontaneous rate would have a slope of exactly 2, according to our earlier analysis. A fibre with a higher spontaneous rate, however, whilst showing the same absolute rate of change, would show a reduced relative rate of change due to the spontaneous activity. On the other hand, a fibre with a spontaneous rate less than zero (as was estimated from the RI function for the unit of Fig. 5, for example) would have a greater relative rate of change at threshold, since the additive constant is negative in this case. Thus the slopes, which range from less than 1 to greater than 4 (Geisler, 1990) may be no more than a simple consequence of the variation in spontaneous rate having a different diluting effect on the normal, absolute slopes.

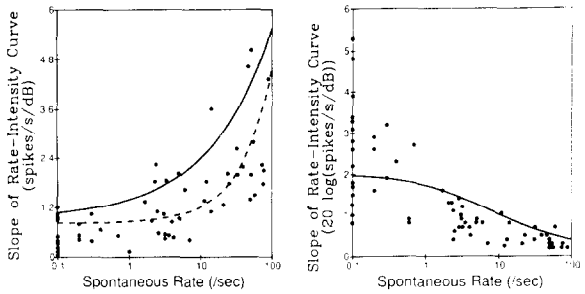

Fig. 8. Slopes of rate-intensity functions at 'tracking threshold' (Geisler et al. 1985). (A) Slopes in absolute terms of spikes/dB. Solid line is the prediction from the analysis given in this paper; dashed line is from the original. The original curve is a closer fit to the lower limit of the data, while the solid line fits better the upper data points. (B) Slopes in relative units, i.e., on a logarithmic scale. Solid line is the prediction from the present paper.

The concept of threshold

The above discussion illustrates the vagueness of the concept of threshold when applied to the auditory nerve. Whether or not thresholds are different between low and high spontaneous-rate fibres depends upon how threshold is defined. If it is defined as a fixed increase in the absolute rate of AP generation then our analysis indicates that there is no difference between fibre types, but if a fixed relative change in firing rates is what defines threshold then low-spontaneous fibres will certainly show thresholds much closer to those of high-spontaneous fibres (although the very concept clearly fails for zero-spontaneous fibres). The physiologically relevant definition will depend upon how the central nervous system uses the information contained in the AP rate code, but relative changes in threshold cannot be useful down to very low spontaneous rates. Detection of a given relative change in AP rate requires the same number of AP events regardless of their rate, and the time required to detect small relative changes may become unrealistically long for low spontaneous fibres.

However, now that the precise shape of the auditory-nerve rate-intensity function is understood at least for the guinea pig and the cat, it is possible to be more rigorous in the definition of threshold. This is true for fibres of almost all spontaneous rates and thresholds at least up to the point at which they might break to take on the sloping-saturation shape. Hence, Eq. 8–9 may be used to define a threshold criterion without ambiguity. For example, our own frequency-threshold tracking algorithm searches for a criterion of approximately $\sqrt{(20^2 + spontaneous^2)}$ spikes/second above spontaneous. If the criterion firing rate increase was halved, the threshold would drop by precisely 3 dB. Regardless of the choice of threshold criterion, so long as it is not too great and does not occur in the sloping-saturation part of the RI curve, it is possible quantitatively to relate the thresholds back to a uniform reference rate.

Nonlinear effects in the cochlea

Dynamic range of cells-vs-the dynamic range of the cochlea

It is clear from our interpretation of the derived BM I/O curves that the mechanics of the cochlea achieves a very significant compression of dynamic range. Specifically, in Figs. 6, 7, 8 and 12 of Yates et al., (1990), we see derived BM I/O curves in which the input stimulus dynamic range of approximately 80–90 dB is compressed into a BM displacement amplitude (output) range of about 30–35 dB. Moreover, the upper 60 dB of input dynamic range changes the BM displacement amplitude by only 12–18 dB. Since IHCs typically have dynamic ranges of approximately 20–30 dB (Russell and Sellick, 1978; Goodman et al., 1982;

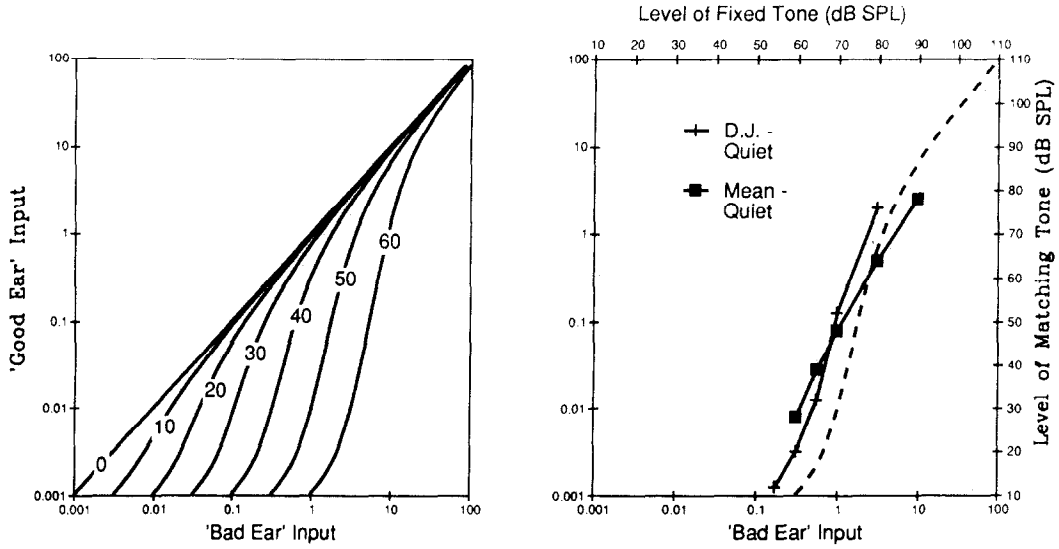

Fig. 9. Recruitment curves extracted from calculations used to generate Fig. 4. Left panel shows calculated differences in input between the curve marked $\beta = 0.999$ in Fig. 4 and the input neccessary to produce the same output calculated for a curve with a different closed-loop gain. The parameter is the effective loss in closed-loop gain, here interpreted as a 'hearing loss'. Right panel shows the 50 dB loss curve plotted against recruitment data measured in a single subject with a unilateral hearing loss of 50 dB, taken from Moore et al., (1985). Also shown (solid squares) are the mean recruitment data from Moore et al.

Patuzzi and Sellick, 1983), this compression of the BM makes it possible for the full stimulus intensity range to be processed by transducer hair-cells which themselves respond over a much smaller dynamic range of BM displacement.

Recruitment

It has been observed in psychoacoustical experiments that cochlear lesions which elevate hearing thresholds are usually accompanied by an increase in the rate at which the perception of loudness increases with stimulus intensity (Pohlman and Kranz, 1924; Moore et al., 1985). The rapid rate of loudness growth usually continues with intensity until the loudness perception reaches the normal value. This property has been called recruitment (Fowler, 1936; Moore et al., 1985), but its cause is unknown. The BM I/O functions and the feedback model suggest a likely explanation.

In Fig. 4 we plotted I/O curves for an electronic model of positive feedback for several values of β, the feedback fraction. We may regard loss of auditory threshold of cochlear origin as being a change in the amount of feedback provided by the active-process (Patuzzi et al., 1989) and therefore calculate the equivalent of a loudness-balance experiment from these data. Fig. 9(left) shows the results. Each curve represents the equivalent of a loudness-balance experiment for a given reduction of β from the value of 0.999. Hence, to calculate the curve labelled 50, which represents the recruitment curve for a loss of 50 dB in the overall loop gain, the following procedure was followed. An output level, say 0.1 volts, was chosen and the input voltage necessary to produce that output was calculated for $\beta = 0.999$, which produced a low-level gain of 60 dB, and for $\beta = 0.684$, the value which produced a gain of 10 dB. These two points were then plotted as the 'Good Ear Input' ($\beta = 0.999$) against 'Bad Ear Input' ($\beta = 0.684$). Repetition for many different values of the output voltage produced the 50 dB recruitment curve.

The curves of Fig. 9 are to be compared directly with psychoacoustic recruitment curves measured by the method of loudness balance (Fowler, 1936). Fig. 9(right) plots one of the curves (50 dB loss) from Fig. 9(left) along with experimental data from Moore et al. (1985) for a single unilaterally deafened subject (subject T.D.) and mean values for 5 subjects. The single subject had

a 50 dB unilateral hearing loss while the mean difference between all pairs of ears was 41.5 dB. The precise details of the match for the single case are obvious: the calculated recruitment curves are an excellent representation in shape and magnitude for the data from the single subject. The match of the mean data, which should be compared with the 40 dB curve since the mean hearing loss was approximately 40 dB, is less precise but this is hardly surprising since averaging many sets of data will conceal the details of individual curves.

The curves of Fig. 9 were calculated using a mathematical analysis of an electronic analogue, not real data from animal experiments. This was, however, for computational convenience only: both the derived and the directly-measured BM I/O curves show the same shape and have been shown to shift, when damaged, in a manner similar to the curves of Fig. 4 (Johnstone et al., 1986). Thus, the general shape of these curves is a good representation of the BM measurements and the argument still holds. The interpretation does, however, rely on accepting that the BM displacement directly determines loudness perception. Another problem with the interpretation of Fig. 9B is that the comparison is made with human subjects for which we have no experimental data on BM nonlinearity.

Two-tone suppression

The auditory nerve response to a probe tone may be reduced by the simultaneous presentation of a second tone of different frequency at a level insufficient to excite the fibre by itself (Arthur et al., 1971; Sachs and Kiang 1968; Sachs 1969). This phenomenon, known as two-tone suppression, has been suggested to result from nonlinear saturation of the active-feedback mechanism by the second tone, thereby reducing the displacement of the BM (Zwicker, 1986; Patuzzi et al., 1989; Geisler et al., 1990). If this were the case, then increasing amounts of suppression of the BM might be analogous to reduction of β in the feedback circuit, as in Fig. 4. Such an interpretation suggests some differential effects on the various RI function types.

We assume, therefore, that the OHC current response to a given BM displacement is reduced by the addition of a simultaneous, second, tone below CF, which drives the OHC into its nonlinear response area. The drive to the active process is therefore reduced and the BM displacement also decreases (Geisler et al., 1990).

We consider separately the response of each fibre type to the simultaneous presentation of a CF probe tone above threshold and a tail-frequency suppressor just below its threshold.

(A) Fibres showing saturating RI functions are associated with the initial linear portion of the BM input-output curve and have reached their maximum firing rate before the break intensity. This part of the BM I/O curve is shifted to the right by a reduction in β, but is otherwise unchanged in shape, and so we might expect a shift in RI functions but little change in shape. In fact, such behaviour is reported (Abbas, 1978; Costalupes et al., 1987; Sokolowski et al., 1989).

By their very nature, however, such fibres are more sensitive to BM displacement and consequently would have lower-than-average thresholds to suppressor tones. In order not to excite such fibres, suppressor tones must be presented at relatively low intensities and this will reduce their suppressive effect on BM displacement. In fact, if both probe and suppressor tones were well below the BM break-intensity it might be expected that they would show little suppression at all.

(B) Sloping-saturation fibres might be expected to be more affected by suppressing tones presented at intensities just below their thresholds. Since their neural responses are less sensitive at all frequencies, choice of a suppressor intensity just below the suppressor's excitation threshold would result in a greater effect on the BM. If the combination of probe and suppressor intensity approached the BM breakpoint intensity then significant suppression of BM displacement would be expected. Thus, sloping saturation fibres should show a greater degree of suppression and a shift to higher intensities. The shift might not be a simple parallel shift, however, since the fibres operate near to the break-point in the BM I/O curve. Above the break-intensity the BM displacement might appear to be somewhat less sensitive to changes in feedback gain and neural responses might be expected to return towards their unsuppressed responses at higher probe levels.

(C) Straight RI fibres should be the most af-

fected by near-threshold suppressing tones. If the suppressor is chosen to be just below the fibre's threshold then it will also be close to or within the BM nonlinearity range and should suppress strongly. The probe tone RI function will shift right at low probe-tone intensities but might be expected to resume its unsuppressed shape at higher intensities, as the effect of the suppressor tone was 'overpowered' by the increasing intensity of the probe tone.

The above discussion relates to suppression as observed with a suppressor just below the suppressor-frequency excitation threshold for that fibre. If, however, we consider the effect on BM vibration of a suppressor tone at fixed intensity then a more global picture emerges. Regardless of the type of fibre considered, a given suppressor tone should produce the same change in vibration on the BM and we should expect the same right shift in probe-tone RI responses. That is, if we consider the suppression effect on BM response then we might expect the same RI shift in all types of fibres, but a differential effect on the shapes of the RI functions.

There is already some indication of these effects in the literature. Schmeidt (1982) showed that suppressor efficacy was closely related to absolute SPL, from which he inferred absolute BM displacement. Fig. 1 of Costalupes et al. (1987) shows a suppressed RI function for a sloping-saturation unit; it exhibits a shift to higher intensities at lower probe intensities but appears to rejoin the unsuppressed RI function at higher intensities. Finally, Sokolowski et al. (1989) show detailed data for fibres of the sloping-saturation type which clearly are not simply right-shifted RI functions.

Conclusions

- It has been shown in an earlier paper that the rate-intensity behaviour of all auditory nerve fibres may be interpreted as an interaction between the nonlinearity of the BM and fibres with a range of BM displacement thresholds, as suggested by Sachs and Abbas (1974). The present paper shows that the saturation feedback model (Zwicker, 1979) adequately explains the form of the nonlinear derived BM input-output functions and that this interpretation leads to a quantitative description of both the directly measured and the derived BM input-output curves.
- An empirical equation which describes the relationships between stimulus intensity and BM displacement, Eq. 9, and between BM displacement and the rate of AP generation in the auditory nerve, Eq. 8, has been shown to describe well almost the full range of auditory-nerve intensity functions, the only exceptions being for some extremely low spontaneous fibres. This function is similar to that of Sachs et al. (1989).
- For all saturating, sloping-saturation and for many straight RI functions the entire range of RI behaviour can be characterised by 5 parameters which may be determined by standard curve-fitting techniques. The exceptions, some extremely low spontaneous rate fibres, do not appear to behave as the other fibres and the difference may be due to saturation of the inner hair cells. The exceptions show different behaviour at both CF and tail frequencies, demonstrating that the differences are not due to the BM nonlinearity.
- The effect of the interaction between BM nonlinearity and the afferent fibres is to extend the dynamic range of the cochlea from the approximately 30 dB of the nerve fibre/synapse combination to something in excess of 70 dB at CF for individual fibres. This apparently is accomplished by a nonlinear, intensity-dependent, amplification which amplifies low-level signals far more than high-level.
- Several physiological properties of normal and pathological processes within the cochlea may be understood in terms of the sloping nonlinearity of the BM and its variation under certain conditions. These include two-tone suppression in normal fibres and recruitment in pathological cochleas.
- Quantitative analysis of rate-intensity functions is now possible, at least in the guinea pig and cat. Since almost all guinea pig RI functions may be described by Eq. 8–9 and straight-forward parameter estimation procedures may be used to determine the best fit to observation, it should be possible to quantify more accurately the results of experiments which rely on RI functions.

Finally, a comment on the engineering aspects of cochlear function. It is common in physiological systems to find negative feedback loops main-

taining operating conditions for various organs within defined boundaries. It is also not unusual in engineering to find the properties of some device being used as a template to define the conditions for a second, similar device which is performing the main function of the system. In the cochlea, however, we appear to have the properties of one set of cells, the OHCs, used in a positive feedback loop simultaneously to amplify weak signals and yet to keep the resultant amplified signals within the operating range of the primary transducers, the IHCs. If the cochlea is to use a dynamic-range compression scheme then it must incorporate a mechanism to keep the operating range correctly adjusted to the operating range of the IHCs. That is, the range-compression mechanism cannot compress the BM displacement into a region which is above or below the displacement amplitudes which best stimulate the IHCs, but must guarantee that the BM displacement is limited to the range which is optimum for the IHCs. The mammalian cochlea seems to have managed this by making the compression scheme directly dependent upon the OHCs, which closely resemble the neural-transduction cells, the IHCs. Since the outer and inner hair cells use a similar current-transduction mechanism (albeit set at slightly different operating points: Cody and Russell, 1987) and the cochlear feedback process causes the BM displacement amplitude to be biased toward amplitudes which lie in the middle of the OHCs operating range, then it is automatically biased to operate in the range which is best for the IHCs.

Acknowledgements

This work was supported by the National Health and Medical Research Council of Australia. I thank Dr O. Gleich and Ms Michelle Thompson for some of the data used in this work, and Drs. B.M. Johnstone, R.B. Patuzzi, D. Robertson and I. Winter for valuable discussions.

Appendix

Calculating the model I / O curves

The simple hyperbolic saturation Eq. 3 leads to a qualitatively satisfactory description of BM input-output functions, but the quantitative agreement is poor. A function is required which has a similar shape but which saturates more suddenly, that is, in which the growth with intensity is linear until closer to the final saturation value. Changing the independent variable x so that it varies as a power of the stimulus input level produced theoretical input-output curves in which the onset of nonlinearity was more abrupt.

The numerical technique was as follows: (a) the shape of the static nonlinearity was defined by specifying a closed-form function (b) The waveform at the input to the amplifier terminals was specified as a sine-wave of a fixed amplitude. (c) The output waveform was then calculated and mapped through the nonlinearity function to define a feedback waveform (which might correspond with the form of the OHC current). (d) The fundamental component of the distorted waveform was extracted by Fourier analysis to represent the output of the feedback loop (modelling the basilar membrane), since it is known that the basilar membrane waveform is a fairly pure sinusoid. The filtered feedback waveform was then subtracted from the input-terminal signal and this gave the value of the applied input signal necessary to produce the calculated output signal. The process is somewhat akin to the technique used to determine neural thresholds: the input necessary to produce a given output is calculated for a range of output amplitudes.

This algorithm was used to explore a number of candidate forms for the feedback nonlinearity.

References

Abbas, P.J. (1978) Effects of stimulus frequency on two-tone suppression: A comparison of physiological and psychophysical results. J. Acoust. Soc. Am. 63, 1878–1886.

Arthur, R.M., Pfeiffer, R.R. and Suga, N. (1971) Properties of two-tone inhibition in primary auditory neurones. J. Physiol. (London). 212, 593–609.

Brophy, J.J. (1983) Basic electrionics for scientists. McGraw-Hill Book Co.

Cody, A.R. and Russell, I.J. (1987) The responses of hair cells in the basal turn of the guinea-pig cochlea to tones. J. Physiol. 383, 551–569.

Costalupes, J.A., Rich, N.C. and Ruggero, M.A. (1987) Effects of excitatory and nonexcitatory suppressor tones on two-tone rate suppression in auditory nerve fibres. Hear. Res. 26, 155–164.

Diependaal, R.J., Viergever, M.A. and de Boer, E. (1986) Are active elements necessary in the basilar membrane impedance? J. Acoust. Soc. Am. 80, 124–132.

Fowler, E.P. (1936) A method for the early detection of otosclerosis. Arch. Otolaryngol. 24, 731–741.

Geisler, C.D. (1990) Evidence for expansive power functions in the generation of the discharges of 'low- and medium-spontaneous' auditory-nerve fibers. Hear. Res. 44, 1–12.

Geisler, C.D., Deng, L. and Greenberg, S.R. (1985) Thresholds for primary auditory fibers using statistically defined criteria. J. Acoust. Soc. Am. 77, 1102–1109.

Geisler, C.D., Yates, G.K., Patuzzi, R.B. and Johnstone, B.M. (1990) Saturation of outer hair cell receptor current causes two-tone suppression. Hear. Res. 44, 241–256.

Goodman, D.A., Smith, R.L. and Chamberlain, S.C. (1982) Intracellular and extracellular responses in the organ of Corti in the gerbil. Hear. Res. 7, 161–179.

Johnstone, B.M., Patuzzi, R. and Yates, G.K. (1986) Basilar membrane measurements and the travelling wave. Hear. Res. 22, 147–153.

Liberman, M.C. (1978) Auditory nerve response from cats raised in a low-noise chamber. J. Acoust. Soc. Am. 63, 442–455.

Moore, B.C.J., Glasberg, B.R., Hess, R.F. and Birchall, J.P. (1985) Effects of flanking noise bands on the rate of growth of loudness of tones in normal and recruiting ears. J. Acoust. Soc. Am. 77, 1505–1513.

Mountain, D.C., Hubbard, A.E. and McMullen, T.A. (1983) Electromechanical processes in the cochlea. In: E. de Boer and M.A. Viergever, (Eds.), Mechanics of Hearing, Martinus Nijhoff Publishers, Delft University Press, The Hague, 119–126.

Neely, S.T. and Kim, D.O. (1983) An active cochlear model showing sharp tuning and high sensitivity. Hear. Res. 9, 123–130.

Neely, S.T. and Kim, D.O. (1986) A model for active elements in cochlear biomechanics. J. Acoust. Soc. Am. 79, 1472–1480.

Palmer, A.R. and Evans, E.F. (1980) Cochlear fibre rate-intensity functions: no evidence for basilar membrane nonlinearities. Hear. Res. 2, 319–326.

Patuzzi, R. and Sellick, P.M. (1983) A comparison between basilar membrane and inner hair cell receptor potential input-output functions in the guinea pig cochlea. J. Acoust. Soc. Am. 74, 1734–1741.

Patuzzi, R.B. and Robertson, D. (1988) Tuning in the mammalian cochlea. Phys. Revs 68, 1009–1082.

Patuzzi, R.B., Yates, G.K. and Johnstone, B.M. (1989) Changes in cochlear microphonic and neural sensitivity produced by acoustic trauma. Hear. Res. 39, 189–202.

Pohlman, A.G. and Kranz, F.W. (1924) Binaural minimum audition in a subject with ranges of definite acuity. Proc. Soc. Exp. Biol. Med. 20, 335–337.

Rhode, W.S. (1971) Observations of the vibration of the basilar membrane using the Mossbauer technique. J. Acoust. Soc. Am. 49, 1218–1231.

Robles, L., Ruggero, M.A. and Rich, N.C. (1986) Basilar membrane mechanics at the base of the chinchilla cochlea. I. Input-output functions, tuning curves, and phase responses. J. Acoust. Soc. Am. 80, 1364–1374.

Russell, I.J. and Sellick, P.M. (1978) Intracellular studies of hair cells in the mammalian cochlea. J. Physiol. 284, 261–290.

Sachs, M.B. (1969) Stimulus-response relation for auditory-noise fibers: two-tone stimuli. J. Acoust. Soc. Am. 45, 1025–1036.

Sachs, M.B. and Abbas, P.J. (1974) Rate versus level functions for auditory-nerve fibres in cats: tone-burst stimuli. J. Acoust. Soc. Am. 56, 1835–1847.

Sachs, M.B. and Kiang, N.Y.S. (1968) Two-tone inhibition in auditory nerve fibers. J. Acoust. Soc. Am. 43, 1120–1128.

Sachs, M.B., Winslow, R.L. and Sokolowski, B.H.A. (1989) A computational model for rate-level functions from cat auditory-nerve fibers. Hear. Res. 41, 61–70.

Schalk, T.B. and Sachs, M.B. (1980) Nonlinearities in auditory-nerve fiber responses to bandlimited noise. J. Acoust. Soc. Am. 67, 903–913.

Schmiedt, R.A. (1982) Boundaries of two-tone rate suppression of cochlear-nerve activity. Hear. Res. 7, 335–351.

Sellick, P.M., Patuzzi, R. and Johnstone, B.M. (1982) Measurement of basilar membrane motion in the guinea pig using the Mossbauer technique. J. Acoust. Soc. Am. 72, 131–141.

Sokolowski, B.H.A., Sachs, M.B. and Goldstein, J.L. (1989) Auditory nerve rate-level functions for two-tone stimuli: Possible relation to basilar membrane nonlinearity. Hear. Res. 41, 115–124.

Teich, M.C. and Khanna, S.M. (1985) Pulse-number distribution for the neural spike train in the cat's auditory nerve. J. Acoust. Soc. Am. 77, 1110–1128.

Winter, I.M., Robertson, D. and Yates, G.K. (1990) Diversity of characteristic frequency rate-intensity functions in guinea pig auditory nerve fibres. Hear. Res. 45, 191–202.

Yates, G.K., Winter, I.M. and Robertson, D. (1990) Basilar membrane nonlinearity determines auditory nerve rate-intensity functions and cochlear dynamic range. Hear. Res. 45, 203–220.

Zwicker, E. (1979) A model describing nonlinearities in hearing by active processes with saturation at 40 dB. Biol. Cybern 35–4, 243–250.

Zwicker, E. (1986) A hardware cochlear non-linear preprocessing model with active feedback. J. Acoust. Soc. Am. 80, 146–153.